Moschonas, I. F. & Kappos, A. J. (2012). Assessment of concrete bridges subjected to ground motion with an arbitrary angle of incidence: static and dynamic approach. Bulletin of Earthquake Engineering, 11(2), pp. 581-605. doi: 10.1007/s10518-012-9395-2

Assessment of concrete bridges subjected to ground motion with an arbitrary angle of incidence: Static and dynamic approach

Ioannis F. Moschonas[1] and Andreas J. Kappos[2]

Abstract. A nonlinear static analysis methodology for the derivation of a set of pushover curves for any angle of incidence of the seismic action (multidirectional pushover curves) for bridges is developed, wherein the interaction between axial force and biaxial moments at critical pier sections or biaxial shear forces at the bearings is taken into account. Dynamic pushover curves (base shear vs. peak deck displacement) for arbitrary angle of incidence of the excitation, are derived for both unidirectional (single-component) and bidirectional (dual-component) ground motion. It is found that neglecting the minor horizontal component leads to underestimation of bridge response, especially along the bridge principal directions and that the angle of incidence of bidirectional excitation affects bridge response, but to a lesser extent than in the case of unidirectional excitation. The proposed procedure is then applied to a straight symmetric bridge, its results are checked against those from response-history analysis, and is found to be sufficiently accurate for practical application. Using the derived results it is also found that the design of the selected bridge is safe since for the design bidirectional earthquake the bridge starts to behave inelastically (the first plastic hinge forms), while its failure occurs for about four times the design seismic action.

Keywords bridges; seismic response; dynamic analysis; pushover analysis; angle of incidence.

1 Introduction

Nonlinear static (pushover) analysis is a widely used tool for the seismic assessment of structures due to its simplicity and the reasonable accuracy that it provides in several cases. For bridges, the simpler case wherein only one horizontal component of the seismic action is considered (single-component seismic action or unidirectional earthquake excitation), acting in the longitudinal or the transverse direction, has been studied considering only the prevailing mode (Fajfar & Gašperšič 1998) or all the significant modes (Paraskeva et al. 2006; Paraskeva & Kappos 2010) in each principal direction of the bridge. The more general case, where the minor horizontal component (dual-component seismic action or bidirectional earthquake excitation) is also taken into account in the analysis of the longitudinal or transverse response, has not been studied to date. It is noted that in the case of buildings, Reyes and Chopra (2011) recently developed a multi-mode procedure (the two horizontal earthquake components act along the building axes). For the general case wherein the ground motion acts at an arbitrary angle, the only available study (Song et al. 2008) proposes a formula for the calculation of critical excitation orientation, utilising the curvatures at the

[1] Research Associate, Department of Civil Engineering, Aristotle University of Thessaloniki, Greece (e-mail: imoschon@civil.auth.gr)
[2] Professor, Department of Civil Engineering, Aristotle University of Thessaloniki, Greece (e-mail: ajkap@civil.auth.gr)

bottom of bridge piers derived by two separate static nonlinear analyses wherein the force vector is parallel to the direction of each principal earthquake component.

In the work presented herein a static nonlinear analysis procedure is developed that leads to the derivation of the pushover curve along any orientation of the earthquake excitation. Repeating the procedure for all selected angles of incidence (e.g. from 0° to 360°, at 15° increments) a set of pushover curves is derived, named 'multidirectional pushover curves'. The term 'multidirectional curves' is suggested for use in describing any type of curves (e.g. dynamic pushover, static pushover, fragility) derived for any orientation of the excitation. In the proposed procedure, the interaction between biaxial moments at critical pier sections, and biaxial shear forces at the bearings, and axial force, i.e. a significant parameter that affects the response of reinforced concrete (R/C) bridges, especially when the earthquake strikes at an arbitrary angle, is taken into account.

Since static nonlinear analysis is an approximation of the actual, dynamic, behaviour, the proposed procedure has to be evaluated against dynamic response-history analysis (RHA). So, at first, multidirectional dynamic pushover curves are derived separately for unidirectional and bidirectional earthquake excitation in order to describe bridge response in terms of base shear vs. peak deck displacement (V-δ) diagrams. The dynamic response of bridges for arbitrary orientation of the bidirectional ground motion has been addressed in some previous studies. Taskari et al. (2008) studied the response of a curved bridge using a deterministic approach, showing that the orientation of the bidirectional earthquake excitation affects bridge response, to a degree depending on the characteristics of ground motion and the considered response quantity. Mackie et al. (2011) recently found that the median lognormal response of straight bridges to a significantly large ensemble of ground motions (a total of 160 records were used) remains practically invariable with the angle of incidence of the dual-component seismic action. The use of such a large number of records is not feasible for practical applications and according to current codes (CEN 2004; 2005) the minimum required number for using the mean response (rather than the most critical one) is seven. In addition, the selected ground motion set in the study by Mackie et al. (2011) is characterised by a uniform distribution of the orientation of the major horizontal earthquake component; hence, the rotation of the major horizontal component is not addressed in investigating the effect of the excitation orientation on bridge response.

The dynamic response of a symmetric straight bridge, subjected to bidirectional excitation is investigated here and compared with the simpler case of the unidirectional earthquake motion. The problem is tackled using the median normal and lognormal response for seven appropriately selected records at two distinct response levels: formation of the first plastic hinge and bridge failure. Then, the proposed procedure is verified against the results of RHA, and is applied to investigate the adequacy of the design of the selected bridge.

2 Methodology for the derivation of multidirectional pushover curves

2.1 Modelling of the seismic action

For a more consistent approach, in lieu of applying the recorded three components of the ground motion, these are transformed into principal components (Penzien & Watabe 1974; Kubo & Penzien 1979) E_I, E_{II} and E_{III} that are linearly independent (or statistically linearly uncorrelated) and directed along a set of principal axes *O-I-II-III*. Components E_I and E_{II} are the horizontal ones, the first one having the maximum intensity (E_I = major, or primary, horizontal component, E_{II} = minor, or secondary, horizontal component).

The simpler approach is to consider only the major horizontal component acting at an angle *a* with respect to the bridge longitudinal axis (Figure 1a). Thus, the axis system *O-I-II-III* is considered identical with system $O\xi\eta\zeta$ which is rotated by an angle *a* with respect to the bridge axes *Oxyz*. Therefore, the major earthquake component E_I acts along $O\xi$ axis and for this reason it will be referred to as E_ξ.

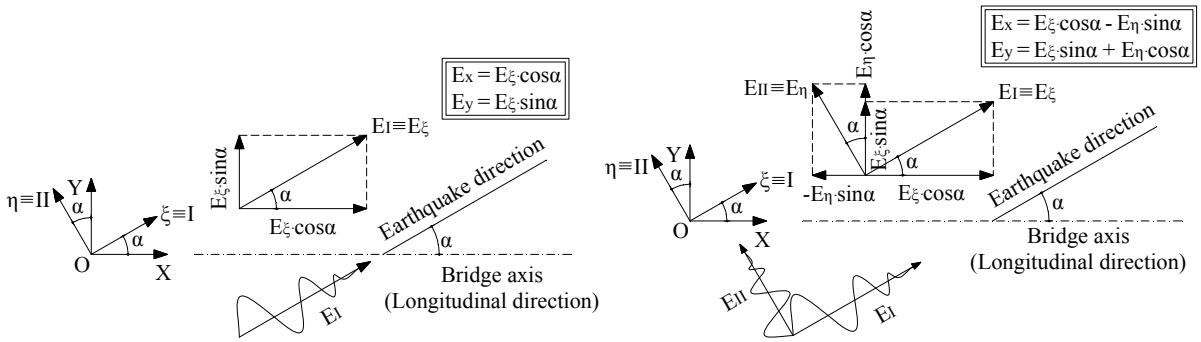

a. Single-component b. Dual-component

Figure 1. Seismic action acting at an arbitrary angle of incidence

The proposed methodology for the derivation of multidirectional pushover curves described in the following section is based on the combination of longitudinal and transverse responses. Therefore, it is more convenient to analyse the major earthquake component into two components $E_x=E_\xi \cdot \cos a$ and $E_y=E_\eta \cdot \sin a$ (Figure 1a) acting along the longitudinal and transverse direction, respectively. Components E_x and E_y have identical time-histories (accelerograms); hence, they are linearly dependent or statistically linearly fully correlated.

For a full treatment of the effect of horizontal ground motion, the minor horizontal earthquake component, $E_{II} \equiv E_\eta$, is also considered (Figure 1b) that is normal to the major horizontal component E_I, which acts at an angle *a* to the longitudinal bridge axis *X* (i.e. the minor component acts at an angle *a* with respect to the *Y*-axis). The components acting along the longitudinal and the transverse bridge directions are $E_x = E_\xi \cdot \cos\alpha - E_\eta \cdot \sin\alpha$ and $E_y = E_\xi \cdot \sin\alpha + E_\eta \cdot \cos\alpha$. These components are a linear combination of E_ξ and E_η, thus they have different time-histories, i.e. they are linearly dependent or statistically linearly correlated. For excitation angles 0°, 90°, 180° and 270°, components E_x and E_y become identical with the principal horizontal components $E_I \equiv E_\xi$ and $E_{II} \equiv E_\eta$, hence they have quite different time-histories, i.e. they are linearly independent or statistically linearly uncorrelated. Conversely, for excitation angles 45°, 135°, 225° and 315°, components E_x and E_y reach their absolute maximum degree of correlation, which, of course, is different for each pair of records.

Only natural earthquake records can be analysed into principal components. Hence, in the case where a code-type response spectrum or spectrum-compatible artificial accelerograms are utilised in the analysis, a proper value for their intensity ratio is required; based on the recent literature (López et al. 2006) a value of 0.70 can be reasonably adopted.

2.2. Derivation of multidirectional pushover curves

Having modelled the seismic action as described previously, the next step in the analysis of concrete bridges is to take into account the interaction between biaxial bending moments and axial force at critical pier sections and/or biaxial shear forces and axial force in the bearings.

To this purpose, the bridge is initially analysed for a low earthquake intensity level wherein the response along both its principal directions remains within the elastic range. Then, the displacements of the selected control point along the longitudinal and transverse directions, $\delta_{L,el}$ and $\delta_{T,el}$, are calculated using elastic response spectra, and from them the corresponding rotations ($\theta_{x,el}$ and $\theta_{z,el}$) and moments ($M_{x,el}$ and $M_{z,el}$) of critical pier sections, as well as the corresponding shear deformations ($\gamma_{x,el}$ and $\gamma_{z,el}$) and horizontal forces ($F_{x,el}$ and $F_{z,el}$) in the bearings along their principal axes, are estimated. The moment ratio $M_{x,el}/M_{z,el}$ (Figure 2) and the bearing shear force ratio $F_{x,el}/F_{z,el}$ remain constant also for higher earthquake intensity levels so long as the loading is monotonically increasing and the response along both principal bridge directions remains elastic. At a certain earthquake intensity level the critical pier section, or an individual bearing, yields under a moment M^{y}_{int} (Figure 2) or force F^{y}_{int}, respectively (the subscript *int* indicates that the point lies on the interaction curve). This means that the critical section or the bearing yields under biaxial conditions earlier than in case wherein the moment vector is normal, or the force vector is parallel, to one of the principal directions. Then, the (idealised as bilinear) M-θ or F-γ diagrams along the principal directions of critical pier sections or bearings are modified using the reduced values of yield moments or yield forces, respectively.

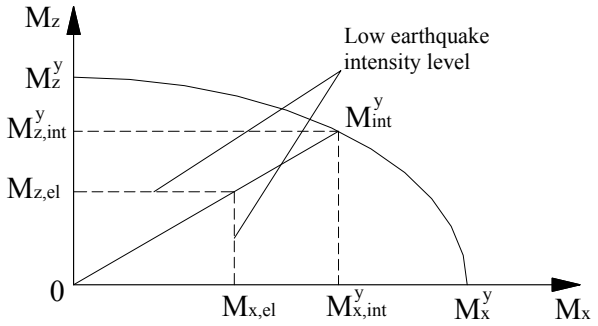

Figure 2. Elliptically idealised moment interaction diagram at a critical R/C pier section

Finally, the selection of an appropriate axis to project the displacement of the control point and the base shear force of the bridge along its principal directions is needed, so that the pushover curve can be plotted. An obvious choice is the axis $O\xi$ of the major earthquake component $E_I \equiv E_\xi$.

The proposed methodology is based on the combination of the responses along the bridge's principal directions to derive the response in the direction of the earthquake, and its successive steps are the following:

Step 1: For a given dual-component seismic action E (code-type spectra or natural records) whose major component acts at an angle a, the corresponding component response spectra E_x and E_y (Figure 1b) are calculated and scaled to increasing levels of earthquake intensity (say, 0.1g, 0.2g,…, $A_{g,u}$·g) until the bridge reaches its ultimate point (bridge failure) at the intensity level $A_{g,u}$ (A_g denoting the normalised peak ground acceleration).

Step 2: For a low earthquake intensity level (e.g. 0.1g), at which bridge response along both its principal directions remains elastic, the moments $M_{x,el}$ and $M_{z,el}$ of critical pier sections and the shear forces $F_{x,el}$ and $F_{z,el}$ of bearings along their principal directions are calculated.

Step 3: The resulting moment ratios $M_{x,el}/M_{z,el}$ and shear force ratios $F_{x,el}/F_{z,el}$ are subsequently used in the corresponding interaction diagrams (Figure 2) to reduce yield moments of critical pier sections and/or yield shear forces of bearings; the reduced values are introduced in the M-θ or F-γ diagrams for the principal directions of critical pier sections and of individual bearings.

Step 4: A 'standard' pushover analysis is performed separately along the longitudinal (0°) and the transverse direction (90°), for lateral force patterns compatible with the corresponding prevailing mode. Then, the derived pushover curves are idealised as bilinear ones (Panagopoulos & Kappos 2009) and they are converted to spectral pushover curves ['capacity curves' (FEMA-NIBS 2003)] of the inelastic equivalent SDOF corresponding to the prevailing mode of each principal direction of the bridge.

Step 5: At each earthquake intensity level the displacement $\delta_{L,max}$ along the longitudinal direction and $\delta_{T,max}$ along the transverse direction are calculated using inelastic or elastic spectra in the region where the equal energy approximation (short period range) or the equal displacement approximation (medium to long period range) is valid, respectively. Then, the corresponding base shears V_{bL} and V_{bT} are extracted from the database of each individual pushover analysis and the projections of these two quantities on the earthquake orientation (Figure 1) are taken, i.e.

$$\delta_{L,proj} = \delta_{L,\max} \cdot \cos\alpha,\ V_{bL,proj} = V_{bL} \cdot \cos\alpha \quad (1)$$

$$\delta_{T,proj} = \delta_{T,\max} \cdot \sin\alpha,\ V_{bT,proj} = V_{bT} \cdot \sin\alpha \quad (2)$$

These projections are combined using an appropriate statistical rule (SRSS, CQC, or ABS), since these response quantities are not simultaneous, for the calculation of the displacement δ_ξ and the base shear force $V_{b\xi}$ in the earthquake orientation. In case the SRSS rule is used, δ_ξ and $V_{b\xi}$ are calculated using the following relationships:

$$\delta_{\xi} = \sqrt{\delta_{L,proj}^2 + \delta_{T,proj}^2} = \sqrt{\delta_{L,\max}^2 \cdot \cos^2\alpha + \delta_{T,\max}^2 \cdot \sin^2\alpha} \quad (3)$$

$$V_{b\xi} = \sqrt{V_{bL,proj}^2 + V_{bT,proj}^2} = \sqrt{V_{bL}^2 \cdot \cos^2\alpha + V_{bT}^2 \cdot \sin^2\alpha} \quad (4)$$

Step 6: Step 5 is repeated for all earthquake intensity levels (0.1g, 0.2g,…, A_{gu}·g) until the bridge reaches its ultimate point in either principal direction. Each pushover curve referring to the earthquake orientation, *a,* is plotted using δ_{ξ}–$V_{b\xi}$ points.

Step 7: Steps 1 to 6 are repeated for all selected orientations (e.g. from 0° to 360° at 15° increments), so multidirectional pushover curves are plotted.

3 APPLICATION TO STRAIGHT BRIDGES

3.1. Description and modelling of the selected straight bridge

The selected bridge (Figure 3) is a 3-span overpass of 71.2 m total length (19.6 + 32.0 + 19.6) that crosses the Egnatia Odos motorway in Northern Greece. The deck is continuous and consists of an 11 m wide prestressed tee section (Figure 4) with two cylindrical voids with 1.10 m diameter. The two piers are 8.5 m high, consist of a solid circular section with a diameter of 1.7 m and are monolithically connected to the deck. The deck movement at the connections with the abutments is free in the longitudinal direction, while in the transverse direction the deck movement is restrained by stoppers, hence resists horizontal forces.

The bridge model used in the present study is similar to the one used by Kappos et al. (2007), ignoring items not relevant to the problem studied herein, such as nonlinearities caused by soil-structure interaction and the activation of the abutment-backfill (ABF) system in both the longitudinal and transverse directions. In the model used here, the ABF system is not modelled in the longitudinal direction, while in the transverse direction only its initial (elastic) stiffness is considered, i.e. it is modelled as a linear spring. A total of 26 frame elements were used, while all the analyses were carried out with the aid of the SAP2000 Nonlinear program (CSI 2009).

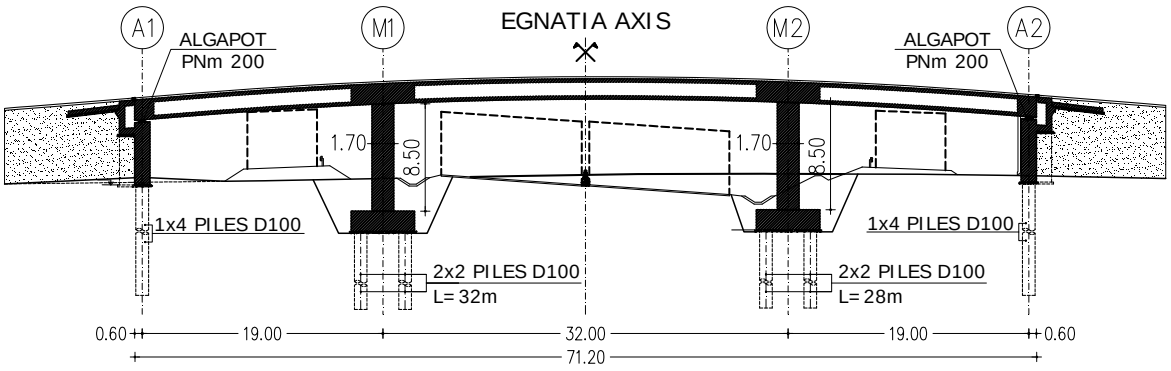

Figure 3. Elevation view of Pedini bridge

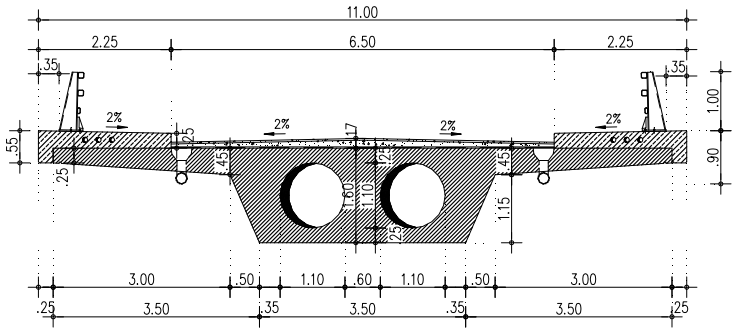

Figure 4. Deck section of Pedini bridge

3.2. Modal analysis of the selected bridge

Modal analysis of the bridge identified two prevailing modes, one for each principal direction (Table 1, Figure 5). The prevailing mode in the longitudinal direction is translational (Figure 5a) and the bridge develops an in-plane deformation, wherein the horizontal displacement vector is parallel to the geometric longitudinal axis (the X-axis). The prevailing transverse mode (Figure 5b) is also translational but the bridge develops an out-of-plane deformation, wherein the horizontal displacement vector is normal to the bridge plane, hence parallel to the geometric transverse axis (i.e. the *Y*-axis). The two prevailing modes define the modal principal axes of Pedini bridge (Figure 6, system *O*-*M*1-*M*2) and they become identical with the geometric principal axes (Figure 6, system *Oxy*), something that is caused by the straight in plan geometry of the selected bridge.

Table 1. Modal characteristics of the two prevailing bridge modes

Prevailing Mode	T [sec]	ε [%]
Longitudinal	0.73	99.8
Transverse	0.92	96.7

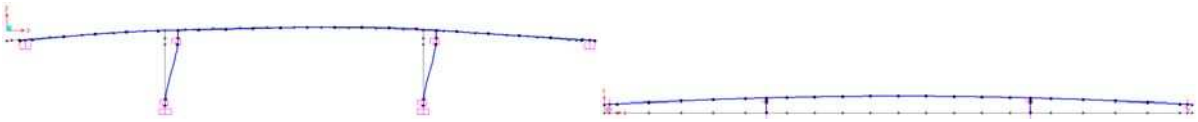

a. Longitudinal b. Transverse

Figure 5. Prevailing modes of the bridge.

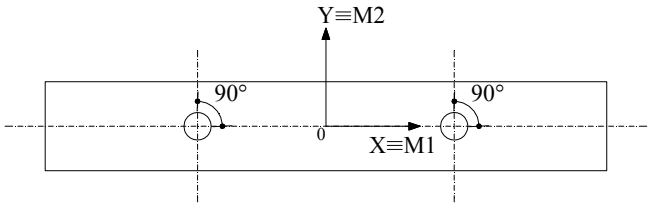

Figure 6. Geometric and modal principal axes of the bridge

3.3. Dynamic analysis for arbitrary angle of incidence

At first, the dynamic response of the selected bridge for different angles of incidence of the bidirectional excitation is investigated in comparison to the simpler case of unidirectional excitation for seven ground motions (Table 2), which have been selected according to the

following procedure: At first, 30 ground motions with magnitude, M, from 5.8 to 6.8 and epicentral distance, R, from 15km to 40km were selected; 5 of them are records from greek earthquakes and they were extracted from the European Strong Motion Database (Ambraseys et al. 2000), while the rest 25 are records from all over the world and they were extracted from the PEER-NGA database (Chiou et al. 2008) using the ISSARS software (Katsanos et al. 2011). Apart from the (M, R) criterion, the similarity of the response spectra of the records and those of the spectrum used for the design of the bridge (A_g= 0.16g, Soil C) was also considered in the selection, while an effort was also made to select records from different earthquakes, to avoid bias in the results. Following the initial selection and the derivation of major and minor principal components, the major component of each of these records was applied along the longitudinal or the transverse axis of the bridge, successively scaled until bridge failure was reached (this corresponded to displacements $\delta_{u,long}$= 0.268 m, $\delta_{u,trans}$= 0.563 m); in this symmetric bridge these displacements correspond to simultaneous exceedance of the available rotational ductility in both piers. All 7-subsets of the 30 motions were analysed and the 7 ground motions of Table 2 were selected that resulted in the minimum coefficient of variation in A_g for unidirectional excitation along either principal bridge direction (COV_{long}= 0.159, COV_{trans}= 0.235); it is noted that A_g is one of the key parameters used later on in studying the effect of angle of incidence. The corresponding response spectra for one of the earthquakes are shown in Figure 7; it is worth pointing out that due to the different frequency content, spectral displacement values for the minor component are higher than those for the major one.

Table 2. Selected ground motions

no.	Shortcut	Earthquake	Station	Date	M	R	Orientation	A_g [g]
1	THESS	Thessaloniki	City Hotel	20/6/78	6.40	29.00	N-S E-W	0.139 0.146
2	AL333	Alkionides (Rec. No. 333)	Corinth-OTE Building	24/2/81	6.70	20.00	N-S E-W	0.359 0.176
3	AL334	Alkionides (Rec. No. 334)	Xilokastro-OTE Building	24/2/81	6.70	20.00	LONG TRANS	0.295 0.154
4	SFN	San Fernando	LA–Hollywood Stor FF	9/2/71	6.61	39.49	N090 N180	0.210 0.174
5	WHN	Whittier Narrows-01	Downey – Birchdale	1/10/87	5.99	15.29	N090 N180	0.243 0.299
6	WMD	Westmorland	Parachute Test Site	26/4/81	5.90	20.47	N225 N315	0.242 0.155
7	CCT	Chi-Chi, Taiwan-03	TCU065	20/9/99	6.20	32.05	N-S E-W	0.282 0.352

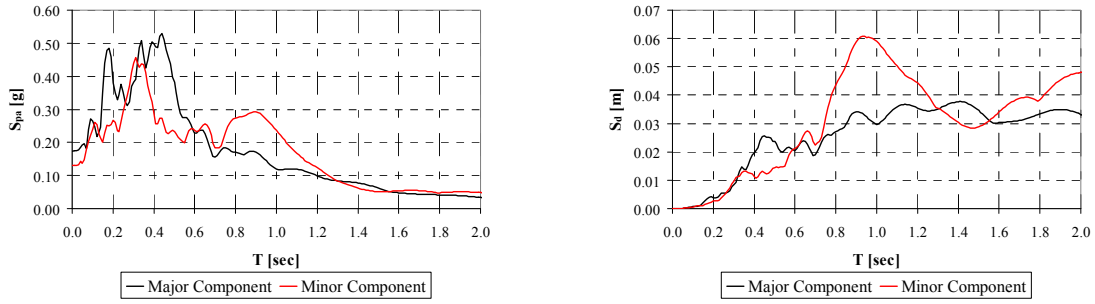

a. pseudo-accelerations b. displacements

Figure 7. Elastic response spectra for principal components of Thessaloniki record

Since the selected bridge is symmetric, it is first checked (as a verification of the procedure) whether its response is also symmetric. Ignoring the moments due to vertical loads and considering only the major principal horizontal component acting at an arbitrary angle, component E_x causes only an in-plane deformation, while component E_y, which has identical time-history but different intensity from that of E_x (see §2.1), causes only an out-of-plane deformation; hence, in the two piers only in-plane or out-of-plane moments are developed, respectively, which have equal value and sign due to bridge symmetry. Therefore, critical sections at the base (and at the top) of the two piers yield simultaneously, therefore bridge response is symmetric. When the minor principal component is also taken into account, components E_x and E_y have different time-histories. Ignoring the moments due to vertical loads, the bridge is initially analysed for the record of Figure 7 acting at an angle a=30° for A_g=0.6g in order to induce inelastic behaviour in both principal directions. The resulting $M(t)$-$\theta(t)$ diagrams at the base and at the top of the two piers along the longitudinal and the transverse directions are shown in Figure 8a and 8b, respectively. In each figure, instead of two $M(t)$-$\theta(t)$ diagrams only one appears, due to their overlapping, which confirms the symmetry in bridge response also in the case of dual-component seismic action. Moments due to vertical loads are ignored in the following discussion, to retain the symmetry in bridge response and allow focussing the investigation on the effect of the excitation orientation.

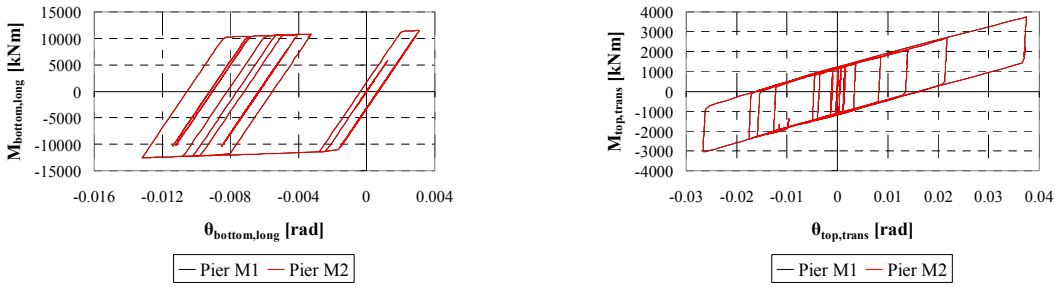

a. Longitudinal direction – Base b. Transverse direction – Top

Figure 8. $M(t)$-$\theta(t)$ diagrams at critical pier sections – Thessaloniki record – a=30°, A_g=0.6g

3.3.1 Dynamic pushover curves

Single-component seismic action is first considered acting along the bridge axes. In Figure 9 the $V_{b,long}(t)$-$\delta_{long}(t)$ loops (labelled 'Dynamic') are shown, resulting from different records, successively scaled until the ultimate point of the longitudinal bridge response is reached

($\delta_{u,long}$ = 0.268 m); as mentioned before, this corresponds to simultaneous exceedance of the available rotational ductility in both piers. Pushover curves for static force distribution consistent with the prevailing longitudinal mode are also plotted on the same figure for the two possible force directions: the positive and the negative, conventionally from left to right and from right to left, respectively. In all cases the pushover curve is found to be identical with the skeleton curve of the $V_{b,long}(t)$-$\delta_{long}(t)$ loops, for either direction. More specifically, both the pushover curves and the skeleton curves are almost bilinear since the M-θ diagrams of the critical pier sections were idealised as bilinear. Hence, when the displacement is maximised the base shear is maximised, as well. The almost bilinear shape of the $V_{b,long}(t)$-$\delta_{long}(t)$ diagrams is due to the fact that yielding occurs almost simultaneously in both piers. The fact that the dynamic envelope coincides with the static (pushover) curves can be explained recalling that the response in the longitudinal direction is fully dominated by the prevailing mode (Table 2). On the other hand, it is observed that the hysteresis loops are highly asymmetric, despite the symmetry of the bridge, since the maximum positive displacement and the maximum positive base shear, are different from the maximum negative ones (in absolute terms); e.g. for the Thessaloniki record (Figure 9a) the maximum displacement in the positive direction does not exceed the yield value, in contrast with the negative displacement which is well into the inelastic range.

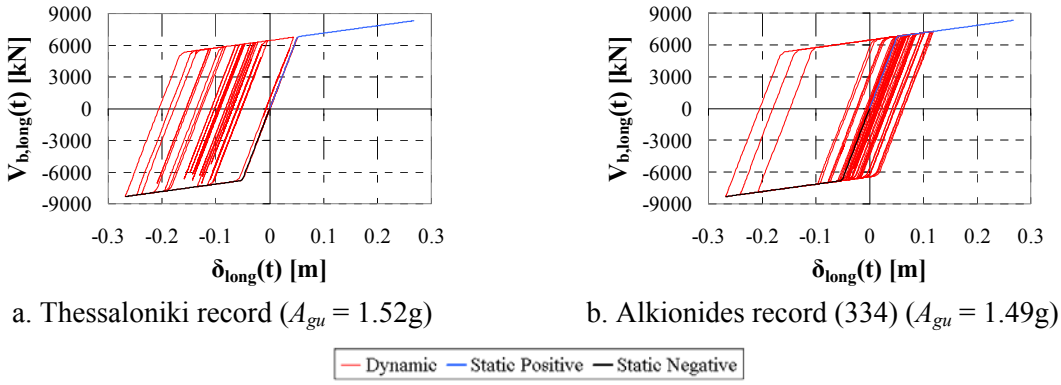

a. Thessaloniki record (A_{gu} = 1.52g) b. Alkionides record (334) (A_{gu} = 1.49g)

Figure 9. Dynamic response of the bridge – Unidirectional excitation – Longitudinal direction

Similar behaviour is expected in the transverse direction, given that this is also dominated by its prevailing mode (which is also the fundamental mode of the bridge, see Table 1). However, the skeleton curves of the derived $V_{b,trans}(t)$-$\delta_{trans}(t)$ loops is not bilinear (Figure 10a). This is attributed to the different response mechanism in the transverse direction, wherein the abutments resist a substantial part of the seismic shear, especially after the yielding of piers, as discussed in more detail by Kappos et al. (2007); this makes the slope of the second branch of the pushover curve just slightly less than the initial one, and makes it also sensitive to the loading history (the location of the contraflexure point in the pier columns varies during the excitation).

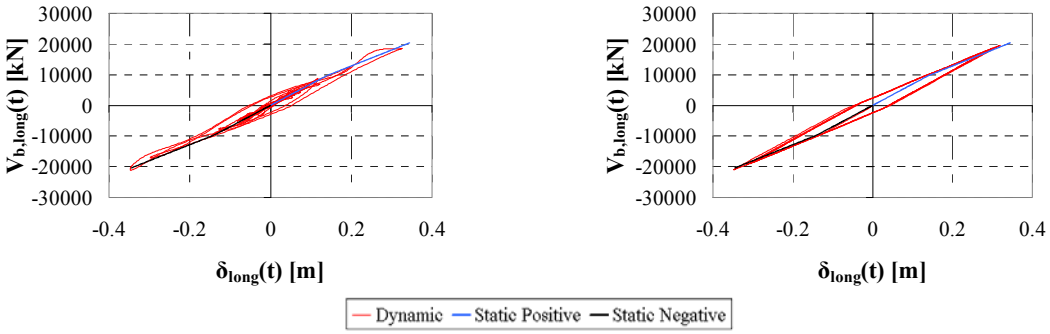

a. Thessaloniki record b. Sine pulse

Figure 10. Dynamic response of the bridge – Unidirectional excitation – Transverse direction

By replacing the actual record with a sine pulse scaled to 0.8g with a period of 2.0 sec, i.e. twice the period of the prevailing transverse mode, 5 loading cycles and a total duration of 5 sec, the derived $V_{b,trans}(t)$-$\delta_{trans}(t)$ diagram (Figure 10b) is now clearly bilinear and, as in the longitudinal direction, its initial loading branch becomes identical with the corresponding static pushover curves in both directions. Therefore, the transverse direction of the selected bridge is more sensitive to the dynamic loading history than the longitudinal one, a feature that cannot be properly captured by a static analysis procedure, such as the one proposed in the present work.he dynamic response of the bridge is then studied for the general case wherein the single- or dual-component seismic action has an arbitrary angle of incidence (a). The representative dynamic pushover curves are defined separately for unidirectional and bidirectional earthquake excitation. In general, there are three different methods to plot the dynamic pushover curves (Mwafy et al. 2001; Kappos & Paraskeva 2008) depending on the values of the control point displacement δ_ξ and the base shear $V_{b\xi}$ along the earthquake axis used for the definition of each $V_{b\xi}$-δ_ξ point: maximum displacement $\delta_{\xi,max}$ vs. simultaneous base shear [hereafter denoted as $\delta_{\xi,max}$-$V_{b\xi}(t_{max\delta})$], maximum base shear vs. simultaneous displacement [denoted as $\delta_\xi(t_{maxV})$-$V_{b\xi,max}$] and maximum displacement vs. maximum base shear [denoted as $\delta_{\xi,max}$-$V_{b\xi,max}$].

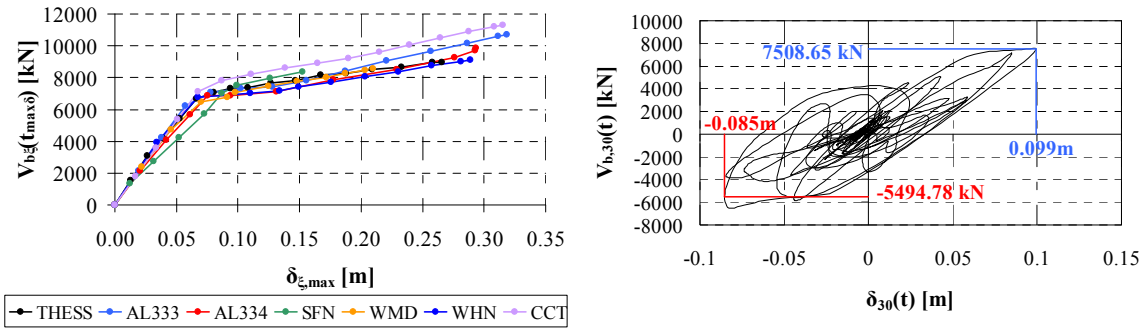

a. Dynamic pushover curves b. $V_{b\xi}(t)$-$\delta_\xi(t)$ diagram – SFN – A_g=0.70g

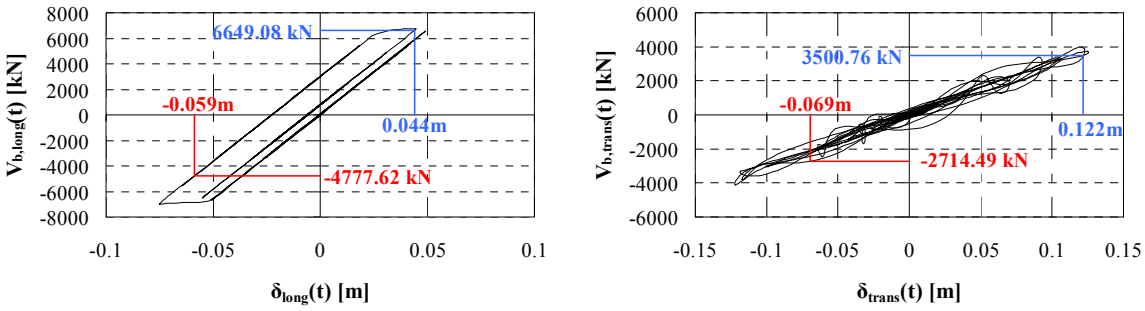

c. $V_{b,long}(t)$-$\delta_{long}(t)$ diagram – SFN – A_g=0.70g d. $V_{b,trans}(t)$-$\delta_{trans}(t)$ diagram – SFN – A_g=0.70g

Figure 11. Dynamic response of the bridge – Unidirectional excitation – a = 30°

Starting from the *unidirectional* excitation in Figure 11a the $\delta_{\xi,max}$-$V_{b\xi}(t_{max\delta})$ pushover curves are shown for all selected ground motions, for a=30°. In all cases the $\delta_{\xi,max}$-$V_{b\xi}(t_{max\delta})$ pushover curves have a 'regular' shape, i.e. the base shear increases with the increment of the maximum displacement, something that can be explained recalling that in unidirectional earthquake excitation the differences between the $V_b(t)$-$\delta(t)$ diagrams along principal bridge directions are caused only by the difference in the bridge's dynamic characteristics, since components E_x and E_y have identical time-histories (see §2.1). Therefore, when δ_ξ is maximum (Figure 11b) displacements along both principal directions are also maximum (Figure 11c and 11d). The simultaneous (with δ_{max}) base shear along the longitudinal direction (Figure 11c) is also maximised, while along the transverse direction it is slightly different from the maximum base shear due to the sensitivity of the transverse direction to the dynamic character of the earthquake loading; hence, $V_{b\xi}(t_{max\delta})$ is practically maximised. Therefore, as also confirmed by the remaining results not shown here, in the case of unidirectional excitation at any angle a, the $\delta_{\xi,max}$-$V_{b\xi}(t_{max\delta})$ pushover curves are representative of the bridge dynamic behaviour.

Moving on to the *bidirectional* excitation (Figure 12a) at an angle a, it is observed that the $\delta_{\xi,max}$-$V_{b\xi}(t_{max\delta})$ pushover curves do not have a regular shape anymore. In the most notable case (San Fernando record), for seismic intensities beyond 0.5g, especially at 0.7g, $V_{b\xi}(t_{max\delta})$ decreases substantially. Recall that unlike the case of unidirectional excitation, here, the difference in the $V_b(t)$-$\delta(t)$ diagrams along principal bridge directions is caused, inter alia, by the significant difference between the time-histories of components E_x and E_y due to the consideration of the uncorrelated minor horizontal component (see §2.1). For this reason, when δ_ξ is maximum (Figure 12b) the corresponding displacements along the principal axes of the bridge are not necessarily maximised (Figure 12c and d); hence, the simultaneous (with δ_{max}) base shear along the principal axes may lie on the unloading or reloading branch of the corresponding $V_b(t)$-$\delta(t)$ diagram. Therefore, $V_{b\xi}(t_{max\delta})$ may be significantly smaller than the value that corresponds to the maximum displacement along each principal axis of the bridge, resulting to the observed drops in strength. The increment in the base shear using its value in a time window $t\pm\Delta t$ instead of its simultaneous value is significantly smaller than the observed strength drop, because of the small time step Δt that it is usually chosen for dynamic analysis, thus using $V_{b\xi}(t\pm\Delta t)$ instead of $V_{b\xi}(t_{max\delta})$ cannot eliminate the 'strength drops'.

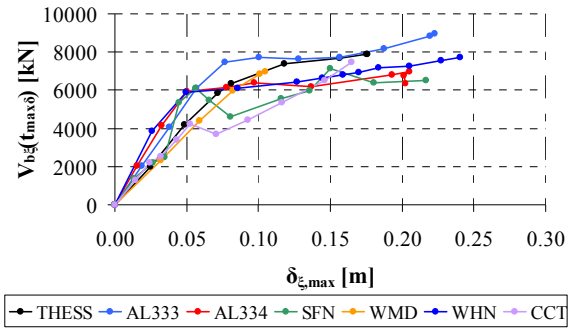

a. Dynamic pushover curves

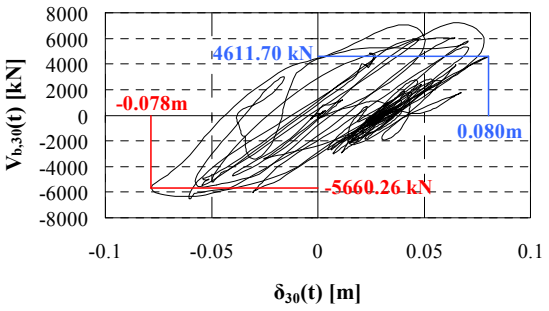

b. $V_{b\xi}(t)$-$\delta_{\xi}(t)$ diagram – SFN – A_g=0.70g

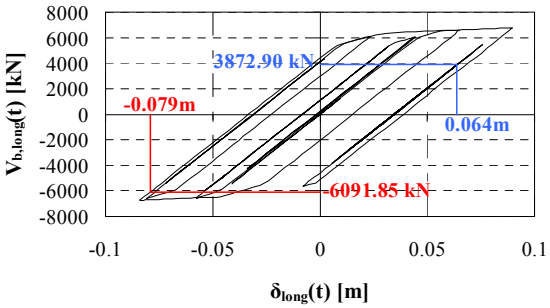

c. $V_{b,long}(t)$-$\delta_{long}(t)$ diagram – SFN – A_g=0.70g

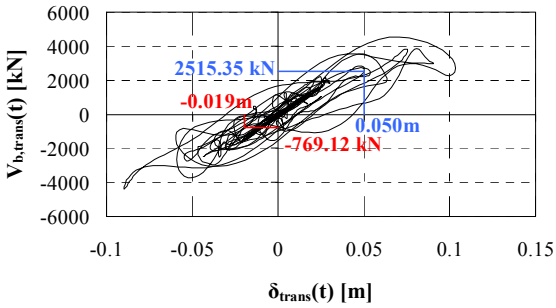

d. $V_{b,trans}(t)$-$\delta_{trans}(t)$ diagram – SFN – A_g=0.70g

Figure 12. Dynamic response of the bridge – Bidirectional excitation, a = 30°

The dynamic pushover curve is a diagram open to different interpretations, its main intended use being to provide a convenient way to compare results from static and dynamic analysis (Mwafy et al. 2001; Kappos & Paraskeva 2008). As discussed previously, it is a realistic representation of the inelastic response when the latter is dominated by the prevailing translational mode, but when the prevailing mode is rotational (Kappos et al. 2011) this is no more the case. Therefore, the most representative dynamic pushover curve for a bridge is not always $\delta_{\xi,max}$-$V_{b\xi}(t_{max\delta})$; a good example is the case of dual-component seismic action where the aforementioned strength drop is noted. Therefore, it is worth checking whether the other two methods for deriving dynamic pushover curves, i.e. $\delta_{\xi}(t_{maxV})$-$V_{b\xi,max}$ and $\delta_{\xi,max}$-$V_{b\xi,max}$ pushover curves, may emerge as more representative. From Figure 13 it is observed that the strength drops in $\delta_{\xi,max}$-$V_{b\xi}(t_{max\delta})$ pushover curves are replaced by strength increments in the $\delta_{\xi}(t_{maxV})$-$V_{b\xi,max}$ pushover curves; thus, none of them provides a meaningful description of the dynamic bridge response. On the contrary, $\delta_{\xi,max}$-$V_{b\xi,max}$ pushover curves have indeed a 'regular' shape, i.e. the maximum base shear increases with the maximum displacement, thus they are deemed as the most representative ones for the case of bidirectional excitation (at an angle).

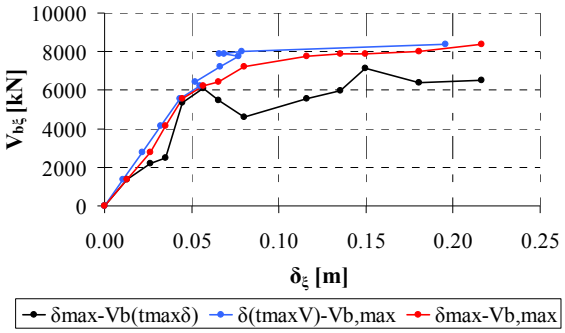

Figure 13. Comparison of the three different methods to plot dynamic pushover curves – San Fernando record (SFN) – Bidirectional excitation, *a*=30°

3.3.2 Effect of angle of incidence

Having defined the representative dynamic pushover curves for the single- and dual-component seismic action, then the corresponding multidirectional dynamic pushover curves are derived for seven angles of incidence of the excitation, from *a*=0° to 90° at 15° increments, separately for each of the 7 selected records for increasing earthquake intensity levels until bridge failure is predicted. A total of 1083 dynamic analyses have been carried out resulting to 7×7×2=98 dynamic pushover curves or equivalently to 14 sets of multidirectional dynamic pushover curves. Figure 14 and 15 show such curves derived using the Thessaloniki and Alkionides (No. 333) records, respectively.

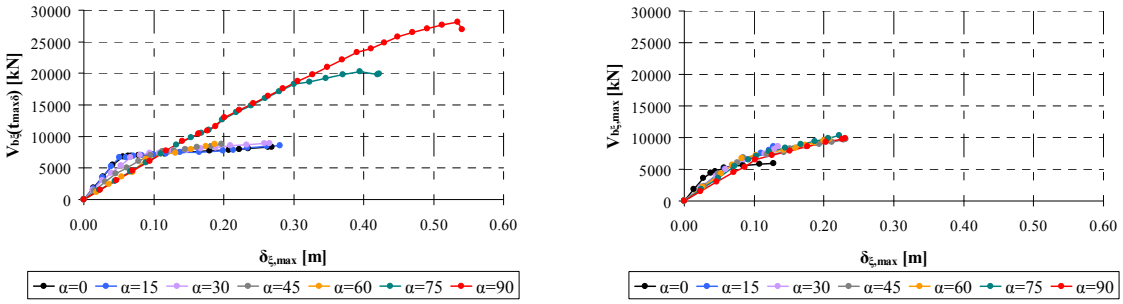

a. Single-component seismic action b. Dual-component seismic action

Figure 14. Multidirectional dynamic pushover curves – Thessaloniki record

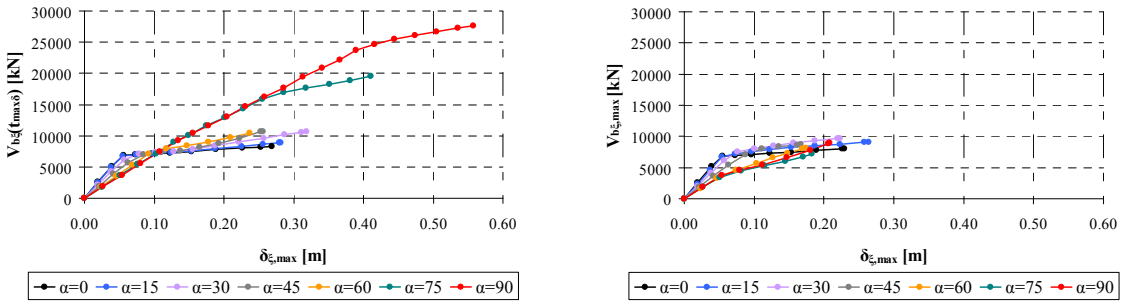

a. Single-component b. Dual-component

Figure 15. Multidirectional dynamic pushover curves – Alkionides record (No. 333)

To facilitate the discussion of results, this is focussed on two distinct response levels: formation of the first plastic hinge and failure (according to the selected ductility criteria). Hereafter these two levels will be referred to as Response Level 1 (RL1) and Response Level 2 (RL2), respectively. The selected response parameter is the deck displacement along the earthquake orientation δ_ξ, and the selected earthquake intensity parameter is the peak ground acceleration A_g.

Table 3. Percentage differences between unidirectional and bidirectional excitation – Dynamic analysis

	1st plastic hinge formation (RL1)				**Bridge failure (RL2)**			
α [°]	**Normal**		**Lognormal**		**Normal**		**Lognormal**	
	$[A_{g,el}]$	**$[\delta_{\xi,el}]$**	**$[A_{g,el}]$**	**$[\delta_{\xi,el}]$**	**$[A_{g,u}]$**	**$[\delta_{\xi,u}]$**	**$[A_{g,u}]$**	**$[\delta_{\xi,u}]$**
0	6.2 (D)	5.0 (D)	6.2 (D)	5.4 (D)	23.4 (D)	22.8 (D)	24.0 (D)	25.6 (D)
15	1.2 (S)	1.4 (D)	0.5 (S)	2.6 (D)	25.8 (D)	26.6 (D)	26.5 (D)	29.4 (D)
30	2.0 (S)	8.6 (S)	0.4 (S)	5.8 (S)	22.1 (D)	28.4 (D)	22.5 (D)	28.7 (D)
45	10.8 (D)	17.6 (S)	11.8 (D)	7.8 (S)	5.5 (D)	11.2 (D)	6.1 (D)	10.6 (D)
60	25.7 (D)	10.4 (D)	25.7 (D)	11.5 (D)	1.3 (S)	15.4 (D)	1.6 (S)	13.1 (D)
75	31.7 (D)	24.0 (D)	31.6 (D)	26.4 (D)	51.4 (D)	52.0 (D)	50.4 (D)	50.5 (D)
90	34.0 (D)	31.5 (D)	33.9 (D)	34.4 (D)	60.8 (D)	58.5 (D)	62.0 (D)	59.9 (D)
most affected	90	90	90	90	90	90	90	90
least affected	15	15	30	15	60	45	60	45

The response of the bridge for arbitrary angle of incidence of the bidirectional earthquake excitation is compared with that to unidirectional excitation. To evaluate the effect of the minor horizontal component on the bridge response, the relative differences in δ_ξ and A_g between unidirectional and bidirectional excitation are given in Table 3 for the selected response levels, RL1 and RL2 and for the median response assuming two common statistical distributions, normal and lognormal. It is observed that in most cases, and at both RL1 and RL2, i.e. over the entire range of bridge response, the values of both parameters (A_g and δ_ξ) are significantly lower when the minor horizontal component is taken into account (the average difference is about 15% for RL1 and 30% for RL2, while the corresponding maxima reach 34% and 62%), something that can also be observed in Figure 14 and 15 with regard to δ_ξ for two individual records. This means that bidirectional earthquake excitation acting at an arbitrary angle, leads to more unfavourable response of the bridge than unidirectional excitation. The most affected direction is the transverse one, because the percentage differences reach their maximum values, i.e. 34% and 62%. In the, generally less critical with respect to bidirectional excitation effects, longitudinal direction, inelastic response (RL2) is much less affected when the minor principal component is taken into account, since increases in δ_ξ vary from 22.8% to 23.4% and in A_g from 24.0% to 25.6%. On the other hand, elastic response (RL1) is practically unaffected, because increases in the two parameters vary from 5.0% to 6.2%. These analyses confirm the intuitive notion that ignoring the bidirectional nature of the ground motion (existence of minor principal component) leads to overestimation of the seismic capacity of the bridge, and reveals as the most critical case that wherein the

major principal component acts along one of the bridge axes (in most cases the transverse one).

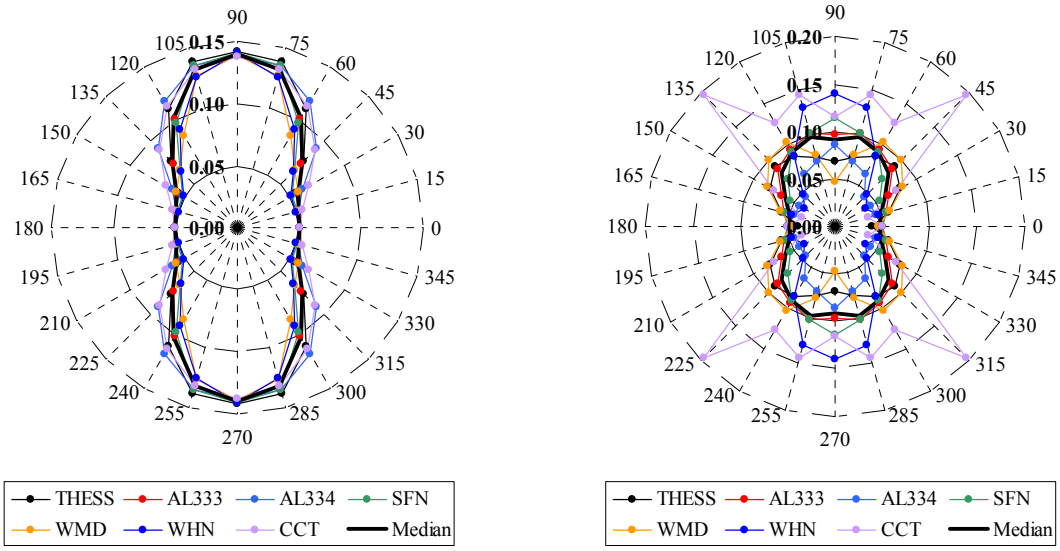

a. Single-component seismic action

b. Dual-component seismic action

Figure 16. Polar diagrams of δ_ξ at first plastic hinge formation (RL1)

To better illustrate the effect of the angle of incidence on the bridge response, polar diagrams of δ_ξ and A_g were plotted for all possible excitation directions, i.e. from 0° to 360° (at 15° increments), in Figure 16 and 18, respectively, for RL1 and in Figure 17 and 19, respectively, for RL2. In addition, the most and the least critical directions for RL1 and RL2 are determined for the single- and the dual-component excitation and the percentage differences between the corresponding peak values (minimum and maximum) of δ_ξ and A_g are given in Table 4 for both statistical distributions assumed (normal and lognormal). The corresponding percentage differences for each record are given in Table 5.

Starting from the unidirectional excitation, the most critical direction (with regard to both A_g and δ_ξ) at RL1 is the longitudinal one (a=0°), while at RL2 the critical angle a=60°. Conversely, the least critical direction (regarding also both A_g and δ_ξ) is the transverse one (a=90°) for both RL1 and RL2. It is noted that the higher resistance in the transverse direction is due to the significant contribution of the abutments, discussed previously; recall that for simplicity of the parametric study, only the linear range of the abutments' response was modelled here; a more detailed, nonlinear model is presented by Kappos et al. (2007). In addition, both critical directions in all cases (i.e. regarding A_g, δ_ξ, RL1 and RL2) are the same for normal and lognormal distribution. Therefore, in the case of unidirectional excitation the most and the least critical orientations are not sensitive either to the input motion characteristics or the assumed statistical distribution.

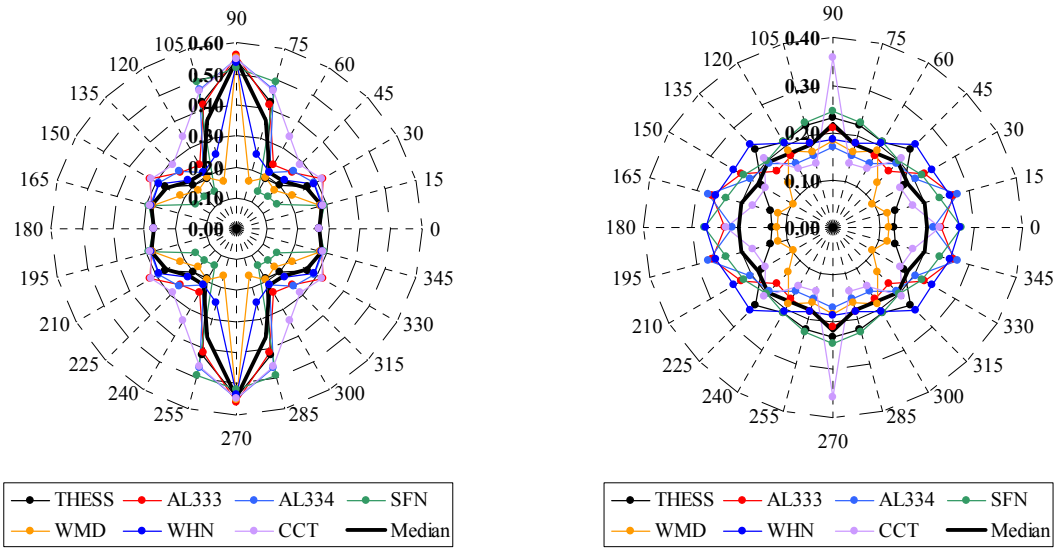

a. Single-component seismic action

b. Dual-component seismic action

Figure 17. Polar diagrams of δ_{ξ} at bridge failure (RL2)

With regard to the bidirectional excitation, the most critical direction at RL1 is also the longitudinal one for both A_g and δ_{ξ}, for both statistical distributions, while at RL2 the critical angle is a=75°. Conversely, the least critical orientation at RL1 is different for A_g and δ_{ξ}, but almost the same, with a small exception with regard to A_g, between normal and lognormal distributions. Similarly, at RL2 the least critical direction is the longitudinal one (a=0°) with regard to A_g and the transverse one (a=90°) with regard to δ_{ξ}, while they are both the same for the two statistical distributions. Therefore, in the case of bidirectional excitation the critical orientations are not sensitive to the assumed statistical distribution, but only the most critical one is not sensitive to the input motion characteristics and to the parameter considered (earthquake intensity or bridge displacement).

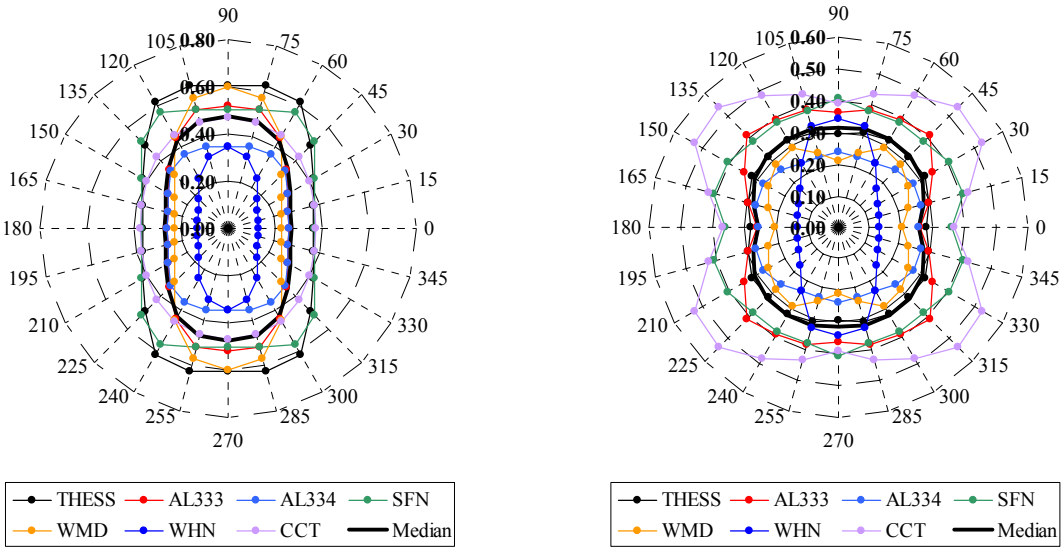

a. Single-component seismic action

b. Dual-component seismic action

Figure 18. Polar diagrams of A_g at first plastic hinge formation (RL1)

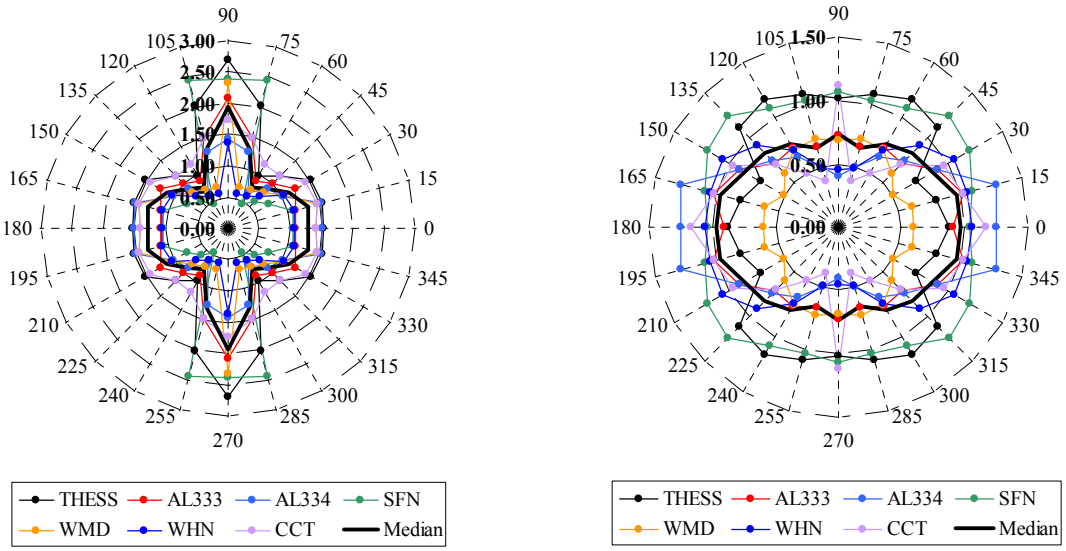

a. Single-component seismic action

b. Dual-component seismic action

Figure 19. Polar diagrams of A_g at bridge failure (RL2)

Regarding the relative differences in δ_ξ and A_g between the most and the least critical directions (another good indicator of the effect of angle of incidence), it is seen in Table 4 that for unidirectional excitation at RL1 the difference is significant, varying from 41.7% to 43.0% for A_g for the two assumed statistical distributions, while it reaches 64.1% for δ_ξ. At RL2 the differences remain significant, varying from 61.1% to 61.7% and from 60.2% to 61.6%, respectively. Hence, the angle of incidence of the unidirectional excitation significantly affects bridge response. For bidirectional excitation, the differences in A_g and δ_ξ are smaller than for unidirectional excitation. More specifically, the differences in A_g vary from 21.4% to 21.5% at RL1 and from 30.1% to 33.1% at RL2. Regarding δ_ξ its peak values vary from 51.2% to 52.6% and from 17.5% to 19.1% at RL1 and at RL2, respectively. Although these differences are smaller than those for single-component excitation, they are still quite

substantial, especially those for A_g, and they are significantly larger for individual records (Table 5), as for example in the case of δ_ξ at RL2, wherein the maximum percentage difference is 61.0% for the Chi-Chi record. Therefore, it appears that when the minor horizontal component is considered, 'directionality' of the excitation is weakened and the effect of the angle of incidence becomes less significant than in unidirectional excitation, then by no means negligible, despite the fact that the code-prescribed number of records was used and the median (normal or lognormal) response at each orientation was considered.

Table 4. Critical directions and percentage differences between the corresponding peak values of A_g and δ_ξ – Dynamic analysis

	Single-Comp.		**Dual-Comp.**		**Single-Comp.**		**Dual-Comp.**	
	[A_g]	**[δ_ξ]**	**[A_g]**	**[δ_ξ]**	**[A_g]**	**[δ_ξ]**	**[A_g]**	**[δ_ξ]**
1st plastic hinge formation (RL1)								
	Median (Normal Distribution)				**Median (Lognormal Distribution)**			
most-crit.	0	0	0	0	0	0	0	0
least-crit.	90	90	45	75	90	90	60	75
Diff. [%]	41.7	64.1	21.4	52.6	43.0	64.1	21.5	51.2
Bridge failure (RL2)								
	Median (Normal Distribution)				**Median (Lognormal Distribution)**			
most-crit.	60	60	75	75	60	60	75	75
least-crit.	90	90	0	90	90	90	0	90
Diff. [%]	61.1	60.2	30.1	19.1	61.7	61.6	33.1	17.5

Table 5. Percentage differences between peak values of A_g and δ_ξ for each record

	Single-Component				**Dual-Component**			
Record	**RL1**		**RL2**		**RL1**		**RL2**	
	[$A_{g,el}$]	**[$\delta_{\xi,el}$]**	**[$A_{g,el}$]**	**[$\delta_{\xi,el}$]**	**[$A_{g,u}$]**	**[$\delta_{\xi,u}$]**	**[$A_{g,u}$]**	**[$\delta_{\xi,u}$]**
THESS	42.1	64.8	64.0	65.5	12.7	56.5	38.8	45.0
AL333	50.3	63.9	57.5	57.6	37.6	50.8	36.3	36.7
AL334	28.8	64.0	58.7	61.2	17.0	50.9	69.0	42.9
SFN	35.4	64.4	81.2	73.8	11.9	56.6	17.1	27.7
WMD	62.3	63.9	70.7	71.3	29.6	55.6	30.2	47.6
WHN	62.7	64.9	57.3	60.9	62.8	73.3	57.7	32.1
CCT	20.5	63.7	32.7	50.8	31.3	81.7	68.2	61.0

3.4. Application and verification of the proposed nonlinear static analysis method

Applying the procedure proposed in §2.2, multidirectional pushover curves were derived separately for each of the selected earthquakes, for seven angles of incidence from a=0° to 90°, at 15° increments. In Figure 20 and 21 the multidirectional pushover curves for the Thessaloniki and Alkionides (No. 333) records are shown.

To evaluate the nonlinear static analysis procedure against dynamic analysis, it is firstly checked whether the former can identify the same basic trends in the bridge response as dynamic RHA. In Table 6 the percentage differences in δ_ξ and A_g between the unidirectional and the bidirectional excitation are given for the two selected response levels. As in dynamic analysis, the differences in δ_ξ and A_g at both response levels are significantly smaller when the minor principal component is taken into account, and the average increase is about 17% for RL1 and 28% for RL2, while the corresponding maxima reach 40% and 48%. These values are slightly different from those in dynamic analysis with the exception of the maximum value at RL2. Therefore, the proposed procedure clearly captures the more unfavourable bridge response under bidirectional excitation. The largest discrepancies are found in the transverse direction, as in dynamic analysis, wherein the decreases in A_g and δ_ξ reach their maximum values, i.e. 40% and 48%. Overall, the proposed nonlinear static procedure is found sufficient for identifying the most affected bridge direction.

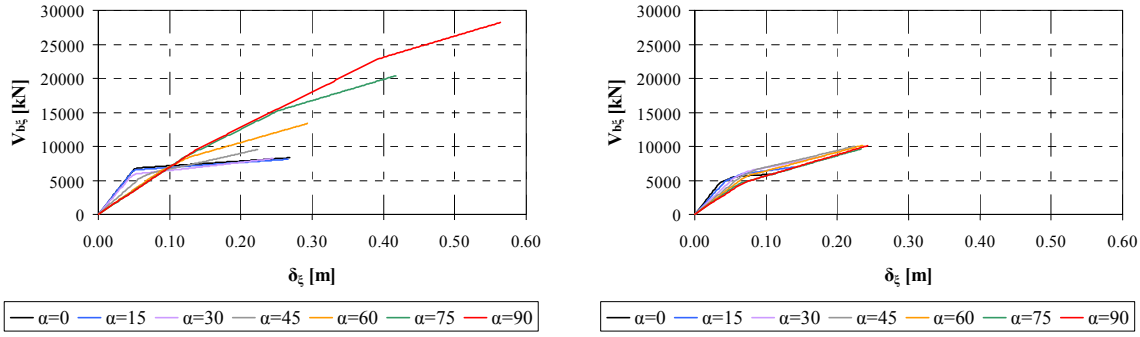

a. Single-component seismic action

b. Dual-component seismic action

Figure 20. Multidirectional static pushover curves – Thessaloniki record

Table 6. Percentage differences between unidirectional and bidirectional excitation – Nonlinear static analysis

	1st plastic hinge formation (RL1)				Bridge failure (RL2)			
α [°]	**Normal**		**Lognormal**		**Normal**		**Lognormal**	
	[$A_{g,el}$]	**[$\delta_{\xi,el}$]**	**[$A_{g,el}$]**	**[$\delta_{\xi,el}$]**	**[$A_{g,u}$]**	**[$\delta_{\xi,u}$]**	**[$A_{g,u}$]**	**[$\delta_{\xi,u}$]**
0	11.9 (D)	10.7 (D)	11.7 (D)	11.2 (D)	27.7 (D)	24.6 (D)	28.0 (D)	27.1 (D)
15	5.9 (D)	4.6 (D)	6.0 (D)	4.7 (D)	27.2 (D)	23.7 (D)	27.1 (D)	25.9 (D)
30	6.6 (D)	9.7 (S)	6.8 (D)	9.4 (S)	29.6 (D)	25.9 (D)	29.3 (D)	16.2 (D)
45	14.3 (D)	9.0 (S)	14.6 (D)	8.6 (S)	18.3 (D)	3.8 (S)	18.4 (D)	3.9 (S)
60	26.8 (D)	12.9 (D)	26.7 (D)	13.1 (D)	26.4 (D)	12.7 (D)	26.3 (D)	12.7 (D)
75	36.5 (D)	31.1 (D)	36.5 (D)	32.6 (D)	37.0 (D)	32.7 (D)	37.0 (D)	33.2 (D)
90	40.8 (D)	38.2 (D)	41.2 (D)	40.8 (D)	48.2 (D)	46.7 (D)	47.8 (D)	47.9 (D)
most affected	90	90	90	90	90	90	90	90
least affected	15	15	15	15	45	45	45	45

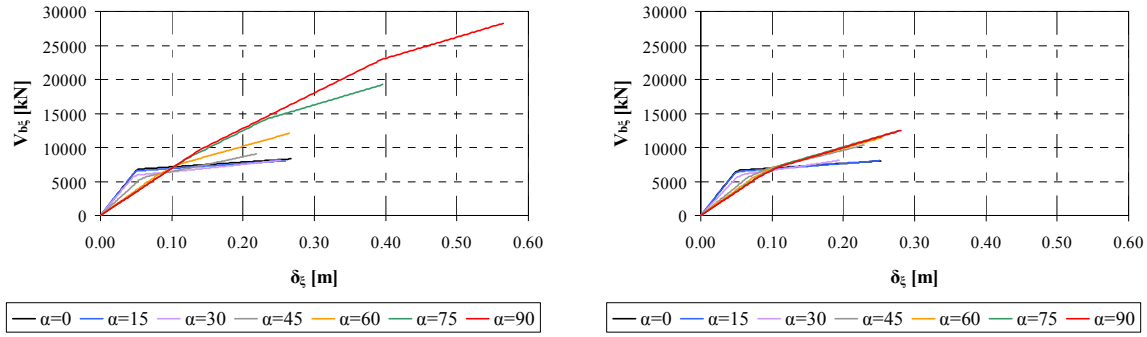

a. Single-component seismic action

b. Dual-component seismic action

Figure 21. Multidirectional static pushover curves – Alkionides record (No. 333)

In Table 7 the most and the least critical angles are listed and the differences between the corresponding peak values of δ_ξ and A_g are given. At RL1, for single-component excitation, the differences in A_g vary from 42.9% to 44.2% for the two assumed probability distributions, while for δ_ξ they are the same, i.e. 66.3%; notably, they are almost the same as the corresponding ones derived from dynamic analysis (Table 4). At RL2, the differences in δ_ξ remain significant, varying from 61.1% to 61.4% (similar to dynamic analysis), while the corresponding differences in A_g vary from 36.3% to 36.5% for the two statistical distributions, i.e. they are smaller than in dynamic analysis; part of this discrepancy is attributed to the use of the equal displacement approximation in estimating target displacements.

For dual-component (bidirectional) excitation the differences in both δ_ξ and A_g are smaller than for single-component, again in agreement with the findings of RHA. More specifically, differences in δ_ξ vary from 45.7% to 47.7% at RL1, and from 34.1% to 34.4% at RL2. Differences in A_g vary from 14.9% to 16.2% and from 12.8% to 14.7% at RL1 and RL2, respectively. Therefore, the proposed procedure correctly identifies the reduced, but still noticeable, effect of the excitation orientation on bridge response when the minor principal horizontal component is included in the analysis.

Table 7. Critical angles and percentage differences between the corresponding peak values of A_g and δ_ξ – Nonlinear static analysis

	Single-Comp.		**Dual-Comp.**		**Single-Comp.**		**Dual-Comp.**	
	[A_g]	**[δ_ξ]**	**[A_g]**	**[δ_ξ]**	**[A_g]**	**[δ_ξ]**	**[A_g]**	**[δ_ξ]**
1st plastic hinge formation (RL1)								
	Median (Normal Distribution)				**Median (Lognormal Distribution)**			
most-crit.	0	30	0	0	0	30	0	0
least-crit.	90	90	90	90	90	90	90	90
diff. [%]	42.9	66.3	14.9	47.7	44.2	66.3	16.2	45.7
Bridge failure (RL2)								
	Median (Normal Distribution)				**Median (Lognormal Distribution)**			
most-crit.	45	45	60	30	45	45	60	15
least-crit.	90	90	15	90	90	90	15	90
diff. [%]	36.3	61.1	14.7	34.4	36.5	61.4	12.8	34.1

Having established that the proposed pushover procedure for arbitrary orientation of the seismic action sufficiently captures the basic trends of the response, its accuracy is further checked against dynamic analysis results, first by focussing on individual records and then by considering the median response, idealising the probability density function as normal or lognormal. To this purpose, peak and average values of the percentage differences in δ_ξ and A_g for each excitation orientation between dynamic analysis and the proposed static nonlinear analysis results are summarised in Table 8, for two of the seven records used [Thessaloniki and Alkionides (No. 333)], and for the median normal and lognormal response resulting from the seven selected records. Starting from the two individual records, at RL1 for unidirectional excitation the maximum differences in δ_ξ and A_g range from 0.1% to 25.9% and from 0.0% to 20.0%, respectively, while their averages range from 11.3% to 11.6%, and from 5.5% to 9.1%, respectively; it is noted that maximum differences occur for an angle of incidence that is different for each parameter considered and for each individual record. For bidirectional excitation the minimum differences in δ_ξ and A_g are larger, varying from 4.0% to 9.3% and from 4.1% to 10.1%, respectively, but maximum differences are similar to those for unidirectional excitation, ranging from 23.7% to 29.8% for δ_ξ, and from 19.9% to 23.4% for A_g. Average values are slightly larger, varying from 16.5% to 21.9% for δ_ξ, and from 12.7% to 15.3% for A_g. Therefore, with regard to the elastic bridge response the proposed procedure produces sufficiently accurate results even when a single ground motion is considered.

Table 8. Differences between nonlinear dynamic and static analysis results

	Single-Comp.		**Dual-Comp.**		**Single-Comp.**		**Dual-Comp.**	
	[A_g]	**[δ_ξ]**	**[A_g]**	**[δ_ξ]**	**[A_g]**	**[δ_ξ]**	**[A_g]**	**[δ_ξ]**
1st plastic hinge formation (RL1)								
	Thessaloniki				**Alkionides (Rec. No 333)**			
Min	0.0	0.5	10.1	9.3	0.5	0.1	4.1	4.0
Max	20.0	23.4	23.4	29.8	12.5	25.9	19.9	23.7
Average	9.1	11.3	15.3	21.9	5.5	11.6	12.7	16.5
	Median (Normal Distribution)				**Median (Lognormal Distribution)**			
Min	0.4	0.4	8.3	5.5	0.5	0.4	8.3	5.7
Max	15.1	22.7	16.3	29.9	14.7	22.5	15.9	21.8
Average	6.8	10.5	12.9	15.5	6.7	10.5	12.5	13.6
Bridge failure (RL2)								
	Thessaloniki				**Alkionides (Rec. No 333)**			
Min	3.0	0.1	2.5	0.2	0.6	0.6	26.0	5.1
Max	42.5	36.3	18.7	12.0	30.7	20.8	40.8	34.0
Average	20.1	9.5	9.2	5.8	17.3	8.4	32.3	20.8
	Median (Normal Distribution)				**Median (Lognormal Distribution)**			
Min	1.8	0.1	7.0	2.5	1.3	0.1	4.3	2.2
Max	39.6	24.6	28.7	35.0	40.8	26.8	31.8	35.1
Average	17.5	8.2	16.5	16.0	17.6	8.8	17.1	16.4

With respect to bridge failure (RL2), for unidirectional excitation the maximum differences are increased compared with the corresponding ones at RL1, and vary from 20.8% to 36.3% with regard to δ_ξ and from 30.7% to 42.5% regarding A_g. The average differences in δ_ξ are similar to those at RL1, ranging from 8.4% to 9.5%, while for A_g they are larger, ranging from 17.3% to 20.1%, attributed to the use of the equal displacement approximation. For bidirectional excitation the maximum differences are larger, as was the case for elastic response, ranging from 12.0% to 34.0% and from 18.7% to 40.8%, for δ_ξ and A_g, respectively. Average differences vary from 5.8% to 20.8% for δ_ξ, and from 9.2% to 32.3% for A_g. Therefore, the proposed procedure produces reasonable results also in the case that the bridge responds inelastically to a specific ground motion.

Referring now to the median normal or lognormal response (hence reducing the uncertainty related to the frequency content of individual ground motions), at RL1 for unidirectional excitation the differences in δ_ξ and A_g are similar to those for the individual record case, varying from 0.4% to 22.7% with an average of 10.5% for δ_ξ and from 0.4% to 15.1% with an average of about 6.8% for A_g. For bidirectional excitation, as in the single record case, the minimum differences in both δ_ξ and A_g are larger, being about 5.5% to 5.7% and 8.3%, respectively, while the maximum (21.8% to 29.9% for δ_ξ and 15.9% to 16.3% for A_g) and the average (13.6% to 15.5% for δ_ξ, and 12.5% to 12.9% for A_g) ones are similar to those for the single component case. Therefore, the use of the median response for the code prescribed number of records does not improve the accuracy of the proposed procedure in the elastic region.

At RL2 (failure), for unidirectional excitation the differences in δ_ξ and A_g are also similar to those for the individual record case, varying from 0.1% to 26.8% with an average of 8.2% to 8.8% for δ_ξ, and from 1.3% to 40.8% with an average of 17.5% to 17.6% for A_g. For bidirectional excitation, as in the individual record case, the minimum differences in both δ_ξ and A_g are larger being 2.2% to 2.5% and 4.3% to 7.0%, respectively, but the maximum and the average differences are similar to those for the individual record case only for δ_ξ (35.0% to 35.1% and 16.0% to 16.4%, respectively). Conversely, the maximum differences in A_g (28.7% and 31.8%) are smaller than those in the single record case; hence, the average differences (16.5% and 17.1%) are smaller than the corresponding ones for individual records. Therefore, the use of the median (normal or lognormal) response in the inelastic region improves the accuracy of the proposed procedure only in the case of the earthquake parameter (A_g), smoothing the effect of the use of the equal displacement approximation.

Having verified the proposed procedure against RHA, its results are then used to compare the bidirectional seismic excitation corresponding to critical levels of the response of the bridge (RL1 and RL2) with the design (elastic) spectrum of Eurocode 8 (CEN 2004) to have an indication of whether the conventional design of the bridge is adequate for any angle of incidence of the ground motion. To this effect, the SRSS spectra of the seven records are scaled separately at RL1 and at RL2, for bidirectional earthquake excitation acting along all selected orientations, and the corresponding average spectra are plotted in Figure 22a and b, respectively, against the SRSS code spectrum for soil class C, and design *PGA* of 0.16g.

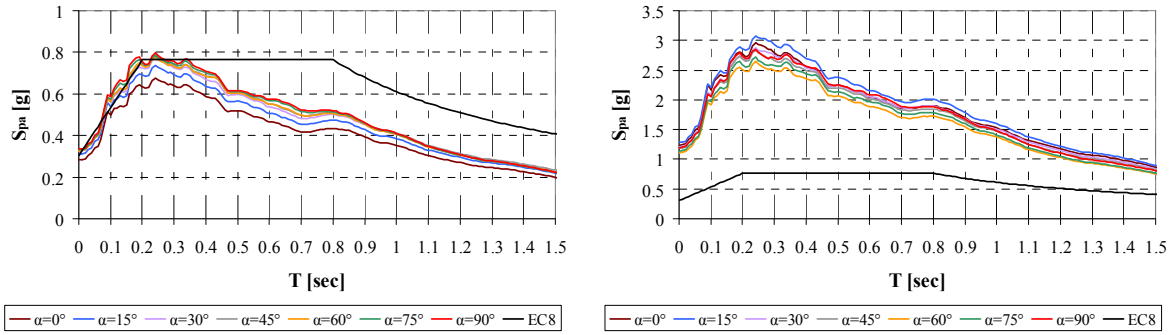

a. RL1 (1st plastic hinge formation) b. RL2 (Bridge failure)

Figure 22. Average spectra of the seven records for bidirectional excitation, for all angles of incidence

It is clear from Fig. 22a that the seismic action causing first yield is generally similar or lower than the design seismic action according to Eurocode 8-Part 2 (CEN 2005). Comparing the peak ground accelerations of the average spectra for bidirectional excitation, $A_{g,av}$, with that of the code spectrum, $A_{g,des}$ it is observed that the ratios $A_{g,av}/A_{g,des}$ vary from 0.93 (for a=0°) to 1.10 (for a=90°); therefore, the design acceleration practically corresponds to the formation of the first plastic hinge at any excitation orientation. Referring to RL2, it is clear that failure of the bridge under bidirectional excitation takes place at earthquake intensity levels substantially higher than the design one; the ratios $A_{g,av}/A_{g,des}$ vary from 3.62 (for a=60°) to 4.21 (for a=15°), confirming the adequacy (and, perhaps the conservatism) of the design of the selected bridge since its failure occurs for an earthquake about four times the design one, for any angle of incidence. Clearly, a more thorough evaluation, including checks of local quantities like member deformations (for which design Eurocode 8 –Part 3 provides design values) would be required for obtaining a more complete picture of the safety margins involved, but is not done here due to space limitations.

4 CONCLUDING REMARKS

From the evaluation of the proposed pushover analysis procedure against the results of dynamic response history analysis, both applied to a simple (yet realistic) bridge configuration, i.e. an existing symmetric straight bridge, it was found that among the various possible types of dynamic pushover curves that can be derived, the most representative ones in the case of arbitrarily oriented excitation are $\delta_{\xi,max}$-$V_{b\xi}(t_{max\delta})$ (i.e. max displacement in the direction of the principal component vs. simultaneous base shear) in the case of unidirectional excitation, and $\delta_{\xi,max}$-$V_{b\xi,max}$ (max displacement vs. max base shear), for bidirectional excitation.

Multidirectional dynamic pushover curves were then derived for a set of seven natural records (transformed into principal components) selected from a larger set by minimising the dispersion in the selected earthquake parameter (here the peak ground acceleration) that results from scaling of the records until bridge failure is reached under unidirectional excitation acting along the bridge principal axes; it is recognised that this is a time-consuming procedure not recommended for ‘code-type’ analysis, but in actual design the simpler

inelastic analysis approach can be adopted, with the code spectrum used for defining the design seismic action. Based on the results obtained, the following basic trends were identified:

- Neglecting the minor principal horizontal component leads to underestimation of the bridge response; this is especially the case when the earthquake acts along the principal axes of the bridge.
- When both principal components are applied, bridge response is still affected by the excitation orientation, but to a lesser extent than in the case wherein only one component is considered; this is attributed to the smoothing of the effect of excitation orientation resulting from the use of a sufficient number of records, since different pairs of records affect differently the response along different angles of incidence.

The proposed nonlinear static procedure was applied to the studied bridge and multidirectional pushover curves were derived. Comparisons with the corresponding dynamic curves have shown that differences between the static and the dynamic approach are generally quite small for the studied key parameters, for both unidirectional and bidirectional input. Hence, the simpler static procedure can be used for studying in a practical context the important effect of arbitrarily oriented seismic input. Further case studies, involving more complex bridge configurations are needed to confirm the trends identified herein.

Finally, selected results from the proposed methodology were used to obtain a first indication of the adequacy of the design of the studied bridge. Comparing the average SRSS spectra of the seven records scaled to the two selected response levels (i.e. formation of the 1st plastic hinge, and bridge failure), the design of the selected bridge was found to be adequate, since for any excitation orientation the bridge remains at the verge of elastic behaviour under the design earthquake, while its failure occurs for an earthquake level about four times the design one.

ACKNOWLEDGEMENTS

The contributions of Asst. Prof. A. Sextos to the modelling of the case-study bridge and of E. Katsanos, Graduate Student at the Civil Engineering Department of the Aristotle University of Thessaloniki, to the selection of the records used in this work are gratefully acknowledged.

REFERENCES

Ambraseys N, Smit P, Berardi D, Rinaldis D, Berge-Thierry C (2000) Dissemination of European Strong-Motion Data. CD-ROM Collection, European Council, Environment and Climate Research Programme.

CEN Techn. Comm. 250 / SC8 (2004) Eurocode 8: Design of structures for earthquake resistance – Part 1: General rules, seismic actions and rules for buildings (EN1998-1). Comité Européen de Normalisation, Brussels.

CEN Techn. Comm. 250 / SC8 (2005) Eurocode 8: Design of structures for earthquake resistance – Part 2: Bridges (EN 1998-2). Comité Européen de Normalisation, Brussels.

Chiou B, Darragh R, Gregor N, Silva W (2008) NGA project strong-motion database. Earthq Spectra 24(1):23-44.

CSI (2009) CSI Analysis Reference Manual for SAP2000®, ETABS®, and SAFE®. Computers & Structures Inc., Berkeley, California.

Fajfar P, Gašperšič P (1998) A simplified nonlinear method for seismic evaluation of RC bridges. In: CD-ROM Proc 6th U.S. Natl Conf on Earthquake Engineering, Seattle, Washington, USA, May 31 - June 4, 1998, Paper No. 23.

FEMA-NIBS (2003) Multi-hazard Loss Estimation Methodology - HAZUS-MH MR4: Earthquake Model Technical Manual. Federal Emergency Management Agency (under a contract with the National Institute of Building Sciences), Washington D.C.

Kappos AJ, Goutzika ED, Stefanidou SP, Sextos AG (2011) Problems in pushover analysis of bridges sensitive to torsion. In: Papadrakakis M, Fragiadakis M, Lagaros ND (eds) Computational Methods in Earthquake Engineering, Springer Science+Business Media B.V., Dordrecht, pp 99-122.

Kappos AJ, Paraskeva TS (2008) Nonlinear static analysis of bridges accounting for higher mode effects. In: Proc Workshop on Nonlinear Static Methods for Design/Assessment of 3D Structures, May 5-6, 2008, Lisbon, Portugal, pp 123-139.

Kappos AJ, Potikas P, Sextos AG (2007) Seismic assessment of an overpass bridge accounting for non-linear material and soil response and varying boundary conditions. In: CD-ROM Proc 1st Int Conf on Computational Methods in Structural Dynamics and Earthquake Engineering (COMPDYN 2007), Rethymno, Crete, Greece, June 13-16, 2007, Paper No. 1580.

Katsanos EI, Sextos AG, Notopoulos T (2011) ISSARS: An Integrated System for Structural Analysis and Earthquake Record Selection. In: CD-ROM Proc 3rd Int. Conf on Computational Methods in Structural Dynamics and Earthquake Engineering (COMPDYN 2011), Corfu, Greece, May 25-28, 2011, Paper No. 224.

Kubo T, Penzien J (1979) Analysis of three-dimensional strong ground motions along principal axes, San Fernando earthquake. Earthq Eng Struct Dyn 7(3):265-278.

López OA, Hernández JJ, Bonilla R, Fernández A (2006) Response spectra for multicomponent structural analysis. Earthq Spectra 22(1):85-113.

Mackie KR, Cronin KJ, Nielson BG (2011) Response sensitivity of highway bridges to randomly oriented multi-component earthquake excitation. J Earthq Eng 15(6):850-876.

Moschonas IF, Kappos AJ, Panetsos P, Papadopoulos V, Makarios T, Thanopoulos P (2009) Seismic fragility curves for greek bridges: methodology and case studies. Bull Earthquake Eng 7(2):439-468.

Mwafy AM, Elnashai AS (2001) Static pushover versus dynamic collapse analysis of RC buildings. Eng Struct 23(5): 407–424.

Panagopoulos G, Kappos AJ (2009) Bilinear idealisation of force - deformation diagrams. In: CD-ROM Proc 16th Hellenic Conference on Concrete, Paphos, Cyprus, October 21-23, 2009, Paper No. 121105 (in Greek).

Paraskeva TS, Kappos AJ (2010) Further development of a multimodal pushover analysis procedure for seismic assessment of bridges. Earthq Eng Struct Dyn 39(2):211-222.

Paraskeva TS, Kappos AJ, Sextos AG (2006) Extension of modal pushover analysis to seismic assessment of bridges. Earthq Eng Struct Dyn 35(10):1269-1293.

Penzien J, Watabe M (1974) Characteristics of 3-dimensional earthquake ground motions. Earthq Eng Struct Dyn 3(4):365-373.

Reyes JC, Chopra AK (2011) Three-dimensional modal pushover analysis of buildings subjected to two components of ground motion, including its evaluation for tall buildings. Earthq Eng Struct Dyn 40(7):789-806.

Song B, Pan JS, Liu Q (2008) Study on critical angle to the seismic response of curved bridges based on pushover method. In: CD-ROM Proc 14th World Conf on Earthquake Engineering, Beijing, China, October 12-17, 2008, Paper No. 14-0120.

Taskari O, Sextos AG, Kappos AJ (2008) 3D finite element modeling of a highway bridge considering the effect of soil and foundation. In: CD-ROM Proc 6th GRACM Int Congr on Computational Mechanics, Thessaloniki, Greece, June 19-21, 2008, Paper No. 1114.